JACS
JOURNAL OF THE AMERICAN CHEMICAL SOCIETY

Article

pubs.acs.org/JACS

A Structure-Based Model of Energy Transfer Reveals the Principles of Light Harvesting in Photosystem II Supercomplexes

Doran I. G. Bennett, Kapil Amarnath, and Graham R. Fleming*

Department of Chemistry, University of California, Berkeley, California 94720

Physical Biosciences Division, Lawrence Berkeley National Laboratory, Berkeley, California 94720

Supporting Information

ABSTRACT: Photosystem II (PSII) initiates photosynthesis in plants through the absorption of light and subsequent conversion of excitation energy to chemical energy via charge separation. The pigment binding proteins associated with PSII assemble in the grana membrane into PSII supercomplexes and surrounding light harvesting complex II trimers. To understand the high efficiency of light harvesting in PSII requires quantitative insight into energy transfer and charge separation in PSII supercomplexes. We have constructed the first structure-based model of energy transfer in PSII supercomplexes. This model shows that the kinetics of light harvesting cannot be simplified to a single rate limiting step. Instead, substantial contributions arise from both excitation diffusion through the antenna pigments and transfer from the antenna to the reaction center (RC), where charge separation occurs. Because of the lack of a rate-limiting step, fitting kinetic models to fluorescence lifetime data cannot be used to derive mechanistic insight on light harvesting in PSII. This model will clarify the interpretation of chlorophyll fluorescence data from PSII supercomplexes, grana membranes, and leaves.

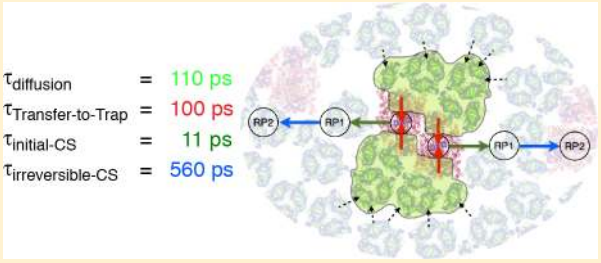

INTRODUCTION

Photosynthesis initiates with the absorption of light by pigments bound to the antenna, or light harvesting, proteins of photosystem II (PSII). The resulting excitation energy is transferred over nanometer distances to the reaction center (RC), where it is converted to chemical energy via charge separation. In plants, the proteins associated with PSII are located in the grana membrane,[1] which is densely packed with photosystem II and major light harvesting complexes (LHCII). PSII reversibly binds with LHCII to form PSII supercomplexes (Figure 1a). PSII supercomplexes and LHCIIs form a large, variably fluid array of pigment−protein complexes.[2] This array forms an energy transfer network that harvests light with 90% efficiency[3] and can respond to changes in incident sunlight intensity and wavelength.[4−6] The largest, structurally well-characterized part of the grana membrane that can harvest light is the PSII supercomplex. A detailed model of this complex would provide access to the blueprint by which PSII efficiently and robustly collects light for photosynthesis.

A complete model of light harvesting in PSII supercomplexes requires both characterizing the kinetics of light harvesting and understanding how the spatial organization of chlorophylls generates these kinetics. Much of the previous work has simplified the complicated kinetics by focusing on potential rate limiting steps to understand the overall process. Two rate limiting steps have been hypothesized for light harvesting in the smallest supercomplex, called the core complex, which has a dimer structure and contains the core antenna proteins (CP43 and CP47) and the reaction center (RC). The excitation radical-pair equilibrium (ERPE) model suggests that excitation will equilibrate throughout the collection of pigments on a time scale much faster than excitation is converted into chemical energy.[7] The ERPE model is, therefore, also known as a trap limited model, since trapping at the RC (via charge separation) is the rate limiting step. The second hypothesis, supported by a computational model of energy transfer in the core complex,[8] assumes a slow rate of transfer between the core antenna proteins and the RC. This hypothesis is known as the transfer-to-trap limited model, where transfer into the RC is the rate limiting step. Fluorescence decay curves measured on the core complex, however, can be fit with either a trap limited or transfer-to-trap limited kinetic model.[9] One experimental study has measured a series of fluorescence decay curves of various PSII supercomplexes.[3] These measurements, when fit to a slightly more detailed kinetic model that incorporated spatial structure, suggested that light harvesting is trap limited. Taken together, the experimental measurements and models of PSII form a conflicted picture of energy transfer and trapping.

Even without knowledge of the detailed kinetics, there have been suggestions about the organizational principle that governs the structure of PSII supercomplexes and results in efficient light harvesting. One possibility is the so-called "energy funnel", in which higher energy chlorophylls are further from the RC.[10] Energy transfer down the gradient would result in unidirectional transport of excitation toward the RC. Previous

Received: April 12, 2013
Published: May 16, 2013

   dx.doi.org/10.1021/ja403685a | J. Am. Chem. Soc. 2013, 135, 9164−9173

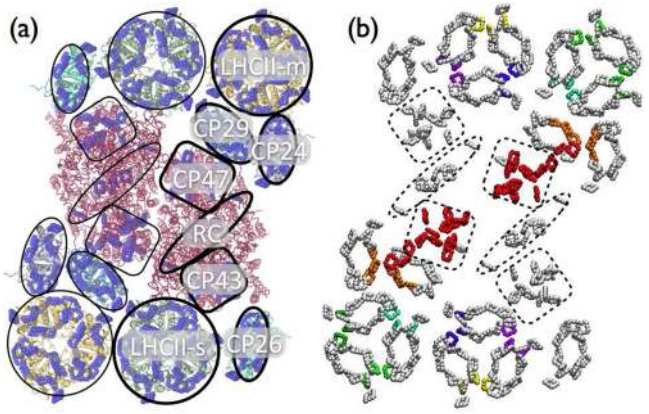

Figure 1. The protein structure and arrangement of $C_2S_2M_2$, the largest isolated supercomplex in plants, are shown based on the structure determined by Caffarri and co-workers.[16] (a) The protein and pigment arrangement are shown. Chlorophylls are represented as blue spheres outlining the chlorin ring. Thick (thin) black outlines surround proteins associated with the right (left) monomer unit of the $C_2S_2M_2$. (b) The protein scaffold has been removed to expose the pigments bound by each protein unit. Pigments belonging to domains contained within a single protein unit are shown in gray. Pigments assigned to a domain delocalized between more than one protein are colored according to their domain assignment.

computational work on PSII core complexes and LHCII trimers, however, suggests that no energy gradient exists in a supercomplex.[8,11] In the absence of an energy gradient, efficient light harvesting in PSII supercomplexes has been attributed to a small collection of fast energy transfer steps forming efficient pathways of energy transfer that extend from the periphery of the supercomplex to the reaction center.[12−14] We call this assumption the pathways model of energy transfer, since it corresponds to assuming that light harvesting in a PSII supercomplex is reducible to a series of energy transfer steps that make up a minimal time pathway from an excited chlorophyll to the RC.[15] Fine-grain population dynamics are not readily accessible to experimental probes, so addressing the organizational principles in PSII supercomplexes requires a structure based model of energy transfer.

With the recent experimental work that resolved the orientations and approximate distances between proteins in the largest PSII supercomplex[16] in plants ($C_2S_2M_2$), it has become feasible to build a structure based model of energy transport for PSII supercomplexes. The number of chlorophylls in a supercomplex (>300 in $C_2S_2M_2$) still makes constructing such a model a daunting computational challenge. We can decrease the computational cost of calculating the rate matrices for a supercomplex and simplify the kinetics of energy transfer by coarse graining over groups of chlorophyll. Such a coarse graining is complicated by the large variations in electronic couplings between pigments. In the presence of small electronic couplings, excitations are localized to single pigments and energy transfer between pigments is caused by electronic coupling. In the presence of strong electronic coupling, excitations are delocalized over multiple pigments and energy transfer between delocalized states is driven by the phonon modes of the bath. While modified Redfield theory interpolates energy transfer rates between both limits of electronic coupling, it does not account for the dynamic localization caused by phonon modes that are strongly coupled to the chlorophyll excited states. Previous work on two components of PSII supercomplexes, LHCII trimers[11,17−20] and the core complex,[8] have used a combined generalized Förster/modified Redfield approach to incorporate an ad hoc correction for the influence of dynamic localization. In the combined approach, chlorophylls are grouped into clusters (called domains) based on the strength of their electronic coupling. In the work of Raszewski and Renger[8] on the core complex, chlorophyll pairs with electronic coupling greater than a threshold value of 34 cm^{-1} were included in the same domain. The treatment of LHCII by Novoderezhkin and co-workers[11] suggested a threshold value of 15 cm^{-1}. No single threshold value will correctly balance electronic delocalization against dynamic localization for all the intermediate couplings in PSII supercomplexes. We, therefore, introduce a method for domain assignment where in cases of moderate to strong coupling the inclusion of a chlorophyll into a domain (or not) is selected on the basis of whether it increases (decreases) the separation of time scales between intra- and interdomain transfer rates. The resulting domains can be used to coarse-grain the energy transfer dynamics by assuming infinitely fast intradomain thermalization.

Using the combined generalized Förster and modified Redfield approach with our separation of time scales metric for domain assignments, we constructed a rate matrix that describes population transport through the chlorophylls bound by PSII supercomplexes. In order to answer questions about the overall kinetics of PSII supercomplexes, we used an effective linearization technique, first introduced by Yang and Fleming,[21] that decomposed the average time scale of light harvesting into contributions from possible rate limiting steps. Next, we calculated photochemical yields in the presence or absence of different domains to assess the appropriateness of the pathways model for explaining the origin of efficient light harvesting by PSII supercomplexes. In both of these discussions, we extrapolate our results to comment on energy transfer and trapping in the membrane. Finally, we show that different mechanistic models of energy transfer fit fluorescence lifetime data equivalently well, which means that quality of fit to data cannot be used as a proxy for physical accuracy of model.

METHODS

This section is divided into three portions. The first explains our approach to treating excitation energy transfer within the pigments of the PSII supercomplex. In this work, we exclude carotenoid molecules from our treatment, and our usage of the term pigment applies only to the chlorophyll *a* (Chl-a), chlorophyll *b* (Chl-b), and pheophytin molecules contained in PSII. Our approach follows previous treatments[8,11,19] in which energy transfer within strongly bound pigment clusters is treated by modified Redfield theory and transfer between clusters is described by generalized Förster theory. The second portion describes the physical parameters we use to model the system including the spatial structure, the interpigment coupling, and site energies. The final portion outlines how we use the calculated rates to construct fluorescence decay spectra and a linearized kinetics model for PSII supercomplexes.

Excitation Energy Transfer Theory. *System and Hamiltonian.* To describe pigment−protein complexes (PPC) containing N pigments, we account for only two electronic states of each pigment: the singlet ground state ($S_0 = |\phi_g\rangle$) and the lowest-lying singlet-excited state ($S_1 = |\phi_e\rangle$). We describe the N-pigment complex with product states shown in eqs 1, 2, and 3 which span the zero-, single-, and double-excitation space, respectively. The higher-order excitation spaces can be constructed analogously. These states are collectively called the site-basis, since they correspond to excitations localized on individual pigments. In the following discussion, μ and γ index the site basis.

dx.doi.org/10.1021/ja403685a | J. Am. Chem. Soc. 2013, 135, 9164−9173

$$|0\rangle = \prod_{i=1}^{N} |\phi_{i,g}\rangle \tag{1}$$

$$|\mu\rangle = |\phi_{\mu,e}\rangle \prod_{\substack{i=1 \\ i\neq\mu}}^{N} |\phi_{i,g}\rangle \tag{2}$$

$$|\mu, \gamma\rangle = |\phi_{\mu,e}\rangle|\phi_{\gamma,e}\rangle \prod_{\substack{i=1 \\ i\neq\mu,\gamma}}^{N} |\phi_{i,g}\rangle \tag{3}$$

In light intensities appropriate for the physiological conditions of photosynthetic PPCs, the excitation energy dynamics sample only the single-excitation space.[22] The single-excitation dynamics are driven by the Hamiltonian (shown here in the site-basis) given in eq 4, where H^{el} contains the electronic vertical-excitation of individual pigments ($\hbar\Omega_\mu$, called the site energy) and the coupling between transitions of pigment pairs ($\hbar J_{\mu,\gamma}$, called the excitonic coupling), H^{el-ph} describes the coupling of the electronic and phonon degrees of freedom, and H^{ph} is the phonon Hamiltonian (within a harmonic oscillator approximation) indexed by ξ.

$$H = H^{el} + H^{el-ph} + H^{ph} \tag{4}$$

$$H^{el} = \sum_{\mu=1}^{N} |\mu\rangle(\hbar\Omega_\mu + \Delta_\mu)\langle\mu| + \sum_{\mu,\gamma} |\mu\rangle\hbar J_{\mu,\gamma}\langle\gamma| \tag{5}$$

$$H^{el-ph} = \sum_{i=1}^{N} |\mu\rangle\hat{u}_\mu\langle\mu| \tag{6}$$

$$H^{ph} = \sum_{\xi} \hbar\omega_\xi(p_\xi^2 + q_\xi^2)/2 \tag{7}$$

The site energy of each pigment is sensitive to changes in the protein configuration that occur on time scales much longer than the time scales of excitation and fluorescence. These long time scale fluctuations are incorporated into the Hamiltonian by adding a random variable Δ_μ that samples a Gaussian distribution with zero mean and a standard deviation of σ_μ. Different values of Δ_μ represent inhomogeneous realizations of the pigments. The electron−phonon coupling is written in terms of the energy gap fluctuation operator ($\hat{u}_\mu$), defined in eq 8, that describes the time evolution of the energy gap between the ground state and excited state harmonic oscillators.[22] We assume that the excited state harmonic oscillator has the same frequency but a displaced equilibrium position ($R^{(0)}_{\mu,e/g}$) with respect to the ground state.

$$\hat{u}_\mu = -\sum_{\xi} \hbar\omega_\xi(R^{(0)}_{\mu,e} - R^{(0)}_{\mu,g})q_\xi \tag{8}$$

Constructing Domains. The largest photosystem II supercomplex contains 324 pigments with the ground and excited states of each coupled to a large collection of phonon modes. The large number of degrees of freedom make it unrealistic to perform a direct calculation of the time evolution of an excitation in PSII with a complete, nonperturbative treatment of the Hamiltonian. Computationally manageable techniques for calculating energy transfer rates in large photosynthetic pigment−protein complexes assume that either the electronic coupling or the electron−phonon coupling can be considered perturbative. In order to use perturbative approaches while still describing the large range of electronic couplings that are found within a PSII supercomplex, we follow a combined approach used previously for treating both the core complex[8] and the major light harvesting complex.[11] In this treatment, chlorophylls are assigned to domains where the electronic coupling between pigments within the domain is assumed to be larger than the electron−phonon coupling, while electronic coupling between pigments in different domains is assumed to be smaller than the electron−phonon coupling. For photosynthetic pigment−protein complexes where there are a wide variety of electronic coupling strengths, no single division of pigments into domains can be considered exact, since many electronic couplings will be comparable in strength to the electron−phonon couplings. In previous work, the separation into domains has been performed by grouping chlorophylls into the same domain when the coupling between them exceeds a threshold value.[8] In this work, we chose to group pigments so as to improve the separation of time scales between inter- and intradomain transfer rates. This choice has the advantage of allowing for a further simplification by coarse-graining over the fast intradomain transfers, a possibility we will explore in the Model of Photosystem II section.

In our treatment, pigments must have coupling above a threshold value[11] (V_{cutoff} = 15 cm^{-1}) and give rise to excitons that rapidly exchange energy to be included in the same domain. Since energy transfer between excitons in the same domain (strong-coupling limit) is driven by site fluctuations, two excitons that have substantial overlap in the site-basis will be rapidly mixed by fluctuations in site energy. This allows excitonic overlap to act as a proxy for energy transfer rates. To calculate this overlap, we removed all coupling in H^{el} less than 15 cm^{-1} and then calculated the transformation matrix ($\tilde{\mathbf{U}}$) associated with this new Hamiltonian. Using the transformation matrix, we calculated the excitonic overlap that two sites experience using eq 9. If the overlap is larger than the threshold value ($S_{\mu,\gamma} > 0.1$, selected to reproduce separation of time scales in LHCII), the two pigments contribute to excitons that exchange energy rapidly. This overlap, however, is also sensitive to the inhomogenous realization, so the two pigments are only in the same domain if $S_{\mu,\gamma} > 0.1$ in at least 50% of all inhomogeneous realizations.

$$S_{\mu,\gamma} = \sum_{m} \frac{\tilde{U}^2_{\mu,m}\tilde{U}^2_{\gamma,m}}{\Phi_m} \tag{9}$$

$$\Phi_m = \sum_{\mu} \tilde{U}^4_{\mu,m} \tag{10}$$

The new hybrid basis ($|M\rangle$) was constructed by forming blocks within H^{el} of the pigments belonging to the same domain and then solving for the eigenvectors of each block ($U_{\mu,M}$). These block-eigenvectors form an orthonormal basis with the property that $\langle M|H^{el}|N\rangle = 0$ if M and N belong to the same domain and M is not equal to N. These vectors do not form an eigenbasis of H^{el}, but they are an eigenbasis within each domain. We then calculated rates of energy transfer within a domain using modified Redfield theory and rates of energy transfer between domains using generalized Förster theory. In the next section, we will present, briefly, the equations that describe the rates of energy transfer in these two cases.

Rates of Population Transfer. The rates of population transfer between excitons in this hybrid-basis ($|M\rangle$) are described by assuming two different limits of coupling. For energy-transfer rates between excitons in different domains (where Dom(M) is the domain of exciton M), we assume a weak interpigment coupling limit where energy transfer is driven by electrostatic interactions, as described by generalized Förster theory. The population transfer rates calculated with generalized Förster theory, shown in eq 11, depend on the absorption and fluorescence spectra ($A_M(t)$ and $F_N(t)$, respectively) of the excitons and the coupling between excitonic states ($|V_{M,N}|^2 = |\langle M|H^{el}|N\rangle|^2$). The real-value components of the Fourier transform of $A_M(t)$ and $F_N(t)$ are the frequency domain line shapes of the absorption and fluorescence spectrum, respectively.

$$k_{M\leftarrow N} = \frac{|V_{M,N}|^2}{\hbar^2\pi}\mathrm{Re}\int_0^\infty \mathrm{d}t A_M(t)F_N^*(t), \quad \text{for Dom}(M) \neq \text{Dom}(N) \tag{11}$$

For energy-transfer rates between excitons in the same domain, we assume a strong interpigment coupling limit where energy transfer is driven by site energy fluctuations (electron−phonon coupling), as described by modified Redfield theory. The population transfer rates between excitons calculated with modified Redfield theory, shown in eq 12, depend on the absorption and fluorescence spectra and a time-dependent coupling, $V_{N,M}(t)$, that describes how the site-energy

dx.doi.org/10.1021/ja403685a | J. Am. Chem. Soc. 2013, 135, 9164−9173

fluctuations induced by phonon modes of the bath couple excitonic states of the same domain.

$$k_{M\leftarrow N} = 2\mathrm{Re}\int_0^\infty \mathrm{d}t A_M(t)F_N^*(t)V_{M,N}(t),$$
$$\text{for Dom}(M) = \text{Dom}(N) \tag{12}$$

A detailed discussion of energy transfer in both the weak and strong interpigment coupling limits is given in the Supporting Information, along with a complete description of the equations that define the absorption/fluorescence spectra and the excitonic couplings appropriate for the generalized Förster or modified Redfield equations.

Boltzmann-Averaged Rates between Domains. The excitation energy transfer rates within a domain are, by construction, much faster than the rate of transfer between domains. This separation of time scales allows for excitation within a domain to thermalize rapidly with respect to transfer out of the domain. The rate of transfer from domain d to domain a is described by eq 13, which performs a sum over the rate of transfer from all the excitons M in d to all the excitons N in a weighted by the Boltzmann population of exciton M ($P_M^{(d)}$).[8]

$$k_{a\leftarrow d}^{\text{dom}} = \sum_{\substack{|M\rangle\in d\\ |N\rangle\in a}} k_{N\leftarrow M}P_M^{(d)} \tag{13}$$

$$P_M^{(d)} = \frac{\mathrm{e}^{-E_M/k_BT}}{\sum_{|M\rangle\in d}\mathrm{e}^{-E_M/k_BT}} \tag{14}$$

Excitation within the supercomplex can then be simplified into a collection of domain populations connected by Boltzmann-averaged rates of transfer. The domain model was found to closely reproduce the full model, as shown in the Model of Photosystem II section, and will be used extensively in this paper because of the computational simplification that it allows.

Constructing Coarse-Grained Models of Energy Transfer. To construct coarse-grained models of energy transfer between compartments composed of many domains, we assumed rapid thermalization within a compartment. These compartments range in size from several domains that incorporate all the chlorophyll in a single protein to 116 domains that incorporate all the chlorophyll in the largest supercomplex ($C_2S_2M_2$). The rates between compartments were calculated using eqs 13 and 14, except the acceptor and donor sites were compartments consisting of several domains. If a domain was shared between two compartments, the domain was put into the compartment containing more chlorophylls assigned to that domain. The low energy domain shared by CP29 and CP24 consists of three chlorophylls from each protein. For the model with protein compartments, this domain was put in the CP29 protein compartment. In the model in which all chlorophylls in PSII form a single compartment, the rate k_{CS} (see the next section) was modified by the Boltzmann population of excitons in the RC domain.

Photosystem II: Parameters. *Structures.* The $C_2S_2M_2$ PSII supercomplex is a 2-fold symmetric dimer (Figure 1a). The supercomplex contains four LHCII trimers and two copies of each of the minor complexes, CP26, CP24, and CP29, as well as two copies of the reaction center core. The structure of the $C_2S_2M_2$ PSII supercomplex was recently obtained at 12 Å resolution.[16] This resolution determined the relative orientations and approximate distances between proteins in the supercomplex. The structure of the reaction center core dimer from cyanobacteria[23] and the structure of the LHCII trimer from spinach[24] have both been solved by X-ray crystallography. We have used a monomer from the LHCII structure for each of the minor complexes. The appropriateness of this substitution is discussed in the Supporting Information. The CP29 crystal structure was recently published,[25] but because there is as yet no Hamiltonian for this protein, we did not use it in our calculations. Still, as discussed in the Supporting Information, the CP29 structure showed high homology with an LHCII monomer, except that Chl 605 in the LHCII monomer has no equivalent in CP29. For this reason, that chlorophyll is deleted in our $C_2S_2M_2$ structure in the LHCII monomer representing CP29. The vertical position of the proteins in the membrane was determined using the Orientations of Proteins in Membranes Database.[26] The lateral orientation was determined using the results of Caffarri and co-workers.[16] The protein structures presented in the paper were generated using the VMD software package.[27] The different supercomplex structures needed to model the fluorescence lifetime data from Caffarri and co-workers[3] were constructed by deleting proteins from the $C_2S_2M_2$ supercomplex. The LHCII trimers within a supercomplex (up to 2 LHCII-s and 2 LHCII-m) are all identical structures with different nomenclature only to identify their positions within the complex.

Hamiltonian. H^{el} is divided into three types of terms: (1) site energies, (2) intraprotein couplings (the interactions of pigments contained within the same protein scaffold), and (3) interprotein couplings (the interactions of pigments contained in different protein scaffolds). The site energies, inhomogeneous distributions, and intraprotein couplings were set to literature values[8,11,28−30] and are reproduced in the Supporting Information. The spectral density, describing the electron−phonon coupling, for each chlorophyll is the same as that used in the original extraction of the site energy. All spectral densities are reproduced in the Supporting Information.

The interprotein couplings were constructed using the dipole−dipole approximation, shown in eq 15, where $\vec{R}_{\mu,\gamma}$ is a vector describing the center-to-center difference in position of the pigments μ and γ. The transition dipole moments are taken from the literature,[8,11,28−30] and their values are reproduced in the Supporting Information.

$$J_{\mu,\gamma} = \frac{\vec{\nu}_\mu\cdot\vec{\nu}_\gamma}{|R_{\mu,\gamma}|^3} - 3\frac{(\vec{\nu}_\mu\cdot\vec{R}_{\mu,\gamma})(\vec{\nu}_\gamma\cdot\vec{R}_{\mu,\gamma})}{|R_{\mu,\gamma}|^5} \tag{15}$$

The use of the ideal-dipole approximation (IDA) to calculate the coupling between pigments in different protein units within PSII assumes that the interprotein distance is large compared to the size of pigments. This is not necessarily the case, since the proteins are quite densely packed inside a PSII supercomplex. TrESP[31] or transition density cube[32] methods could be used to describe the nondipole terms that arise when two charge distributions interact at distances comparable to their size. We have not used a more elaborate technique to quantify interprotein couplings in PSII supercomplexes because of concerns about the remaining uncertainty in the spatial structure. As higher resolution structures become available, improved descriptions of the interprotein couplings should be applied to supercomplexes.

Electron Transfer Scheme. A detailed model of excitation and electron transport within the reaction center presented by Novoderezhkin and co-workers[33] proposed that charge separation can be initiated through either the excited states of special pair ($P_{D2}^*/P_{D1}^* \rightarrow P_{D2}^+P_{D1}^-$) or the associated D1 chlorophyll ($Chl_{D1}^* \rightarrow Chl_{D1}^+Phe_{D1}^-$). The electron transport scheme contains 5 different charge separated populations with 11 rate constants. Novoderzhkin and co-workers used pump−probe data to parametrize their electron transfer model. In this work, we will be simulating fluorescence decay curves which are only sensitive to the coarse features of energy transfer. As such, we decreased the number of fit parameters associated with our model. We chose to describe the electron transport scheme phenomenologically by including only two radical pair states. The two states (RP1 and RP2) and three kinetic rates that define the electron transfer process in our model are shown in Figure 2. The radical pair states RP1 and RP2 do not have direct physical interpretation in terms of molecular charge separated states. Instead, the kinetic rates and

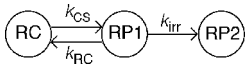

Figure 2. Charge separation scheme. RC represents the reaction center domain, which contains four chlorophyll (two special pair and two associated chlorophyll) and two pheophytin. Each reaction center in a PSII supercomplex performs electron transfer using the same rate constants.

dx.doi.org/10.1021/ja403685a | J. Am. Chem. Soc. 2013, 135, 9164−9173

populations describe the overall behavior of charge separation without assuming any particular molecular identity for the electron transport intermediates in the reaction center. The three kinetic rates (k_{CS}, k_{RC}, and k_{irr}) describing electron transfer were determined by fitting the experimental fluorescence decay spectra with simulated curves.

Simulating Fluorescence Decays. The master-equation formalism (eq 16) defines energy transfer in terms of the rate matrix ($\mathbf{K}$) which contains the transfer rates between excitons or domains and the transfer rates from the RC to the charge separated states and the population vector ($P(t)$) describing the distribution of excitation at a given time. Additional loss pathways in the form of radiative (k_{fl}) and nonradiative (k_{nr}) are also present in the system and are treated explicitly as additional compartments within the kinetic model. The fluorescence rate of each exciton was scaled by its transition dipole moment squared with the average fluorescence time scale across all states of the system set to 16 ns.[34,35] The nonradiative rate was assumed to be equal for all excitons with a time scale of 2 ns.[34,36]

$$\dot{P}(t) = \mathbf{K}P(t) \tag{16}$$

The fluorescence decay spectra were calculated as a function of the initial excitation by projecting into the basis of the eigenvectors of the rate matrix ($|u\rangle$), as shown in eqs 17−19.[37] The decay time scales (τ_u) are the inverse of the uth eigenvalue of the rate matrix, the fluorescence weight factor ($0 \leq \tilde{k}_m^{fl} \leq 1$) is the relative fluorescence rate of each exciton, and the similarity transform matrix (Θ^{-1}) projects from excitons ($|M\rangle$) to the eigenvectors of the rate matrix ($|u\rangle$).

$$F(t) = \sum_M \tilde{k}_M^{fl} \langle M|e^{Kt}|P(0)\rangle \tag{17}$$

$$= \sum_u a_u e^{-t/\tau_u} \tag{18}$$

$$a_u = \sum_M \tilde{k}_M^{fl} \langle M|\Theta|u\rangle\langle u|\Theta^{-1}|P(0)\rangle \tag{19}$$

Since experimental measurements of fluorescence lifetimes using time-correlated single photon counting have finite resolution, we have implemented resolution loss by setting a lower limit to lifetime components (τ_u) of 8 ps. Any amplitude a_u associated with a lifetime less than the lower limit is shifted up to 8 ps.

Calculating Linearized Kinetics. To analyze the rate limiting steps for trapping within PSII, we have chosen to calculate a decomposition of the average trapping time in terms of a hierarchical linearization of the overall kinetic rate matrix. Following the work of Yang and Fleming,[21] the average trapping time can be described using a sequence of rate matrices ($\mathbf{K}_i$) and kinetic compartments (σ_i) constructed to satisfy the condition that the ith kinetic compartment is a perfect trap within the $\mathbf{K}_{i+1}$ rate matrix. RP2 is a trap for the entire rate matrix, so we begin by defining σ_0 = RP2 and $\mathbf{K}_1$ is the domain rate matrix, composed of thermal transfer rates between domains. Subsequent kinetic compartments and rate matrices are defined in terms of eqs 20 and 21.

$$\mathbf{K}_i = \mathbf{K}_{i-1} - \mathbf{K}_{i-1}|\sigma_{i-1}\rangle\langle\sigma_{i-1}| \quad \text{for} \quad i \geq 2 \tag{20}$$

$$\langle\sigma_i| = \langle\sigma_{i-1}|\frac{\mathbf{K}_i}{\sqrt{\langle\sigma_{i-1}|\mathbf{K}_i\mathbf{K}_i^T|\sigma_{i-1}\rangle}} \tag{21}$$

The effective forward transfer time ($\tau_{i\leftarrow i+1}^{eff}$) is the average time for transfer from kinetic compartment i+1 to kinetic compartment i in the presence of back-transfer away from the final charge separation state (RP2). The complete expressions for calculating the effective forward transfer times are presented in the Supporting Information. The average trapping time is determined by both the effective rates of transfer along the chain of kinetic compartments and the initial population of excitation within the system. The contribution of $\tau_{i-1\leftarrow i}^{eff}$ to the average trapping time is weighted by ρ_i, the fraction of population initiated in compartments $j \geq i$.

$$\tau_{trap} = \sum_{i=0}^{N_{max}} t_{i-1\leftarrow i} \tag{22}$$

$$t_{i-1\leftarrow i} = \tau_{i\leftarrow i+1}^{eff}\rho_{i+1} \tag{23}$$

$$\rho_i = \sum_{j=i}^{N_{max}} P_j(t=0) \tag{24}$$

MODEL OF PHOTOSYSTEM II

Pigment Domain Assignments Reveal Inter-Protein Domains. Photosystem II pigments (Chl-a, Chl-b, and pheophytin) were grouped into clusters of strongly interacting pigments called domains. While it is often assumed that pigments will interact most strongly with other pigments bound within the same protein,[38,39] we have used the supercomplex structure to assign domains with an unbiased approach that depends only on the couplings and energy gaps of the relevant chlorophylls. This method has revealed a small set of pigments that form domains delocalized across multiple proteins. Figure 1b shows the $C_2S_2M_2$ supercomplex with the protein scaffold removed to display only the pigments. Chlorophylls belonging to a domain delocalized over more than one protein unit are shown in colors according to their domain assignment. Within LHCII trimers, we see delocalization between high energy pigments belonging to different monomers (e.g., the yellow, blue, and purple chlorophylls bound by LHCII-s). CP24 and CP29 share a domain that contains the lowest energy exciton of both proteins (the orange chlorophyll). Additionally, CP29 has two pigments that belong in the same domain as 15 of the 16 CP47 chlorophylls (the red chlorophylls). The remainder of the chlorophyll (shown in gray) have the same domain assignments within a $C_2S_2M_2$ supercomplex as they would in an isolated protein.

Testing Infinitely Fast Intra-Domain Equilibration. The domain assignments used in this work were selected to increase the separation of time scales between inter- and intradomain transfer rates. In the limit that a complete separation of time scales is achieved, the much faster intradomain rates will result in excitation energy thermalizing prior to transfer out of the domain. We constructed a new rate matrix (domain model) that coarse-grains the system at the domain level by assuming infinitely fast intradomain thermalization. To assess the error associated with this domain model, we calculated the domain populations as a function of time both with and without assuming infinitely fast equilibration within domains. For these calculations, electron transfer in the RC is treated as infinitely fast and irreversible. To assess the similarity of the dynamics in both cases, we calculate two error metrics $\Delta_{max}^{(d)}$ and $\Delta_{Integral}^{(d)}$. $\Delta_{max}^{(d)}$ measures the maximum absolute deviation of the two population traces as a percentage of the maximum population of the domain calculated with the full rate matrix. The second metric, $\Delta_{Integral}^{(d)}$, reports the integral of the absolute deviation over all time as a fraction of the integral of the population calculated using the full rate matrix over all time. The mathematical expressions for these terms are described in the Supporting Information.

No matter what domain is initially excited, we found that $\Delta_{max}^{(d)} < 2\%$ and $\Delta_{integral}^{(d)} < 7\%$ for all domains of $C_2S_2M_2$. The population curve with the largest error in both of these measures is shown in Figure S1 of the Supporting Information. The difference between the dynamics calculated with the full

dx.doi.org/10.1021/ja403685a | J. Am. Chem. Soc. 2013, 135, 9164−9173

rate matrix versus the domain rate matrix in this plot is barely differentiable by eye. The excellent agreement between the domain model and the full calculation supports our method for assigning chlorophylls to domains using a separation of time scales metric. We have used the domain model as the reference calculation for the remainder of the paper.

Extracting Electron Transfer Rates. The fluorescence lifetime of a PSII supercomplex is determined by both the rates of energy transfer in the antenna and electron transfer kinetics in the reaction center. We incorporated the electron transfer rates (shown in Figure 2) into the domain model and extracted their values by fitting fluorescence decay spectra. In previous work, Caffarri and co-workers[3] measured fluorescence decay spectra collected from five bands separated using sucrose density gradient centrifugation on thylakoid membranes. These bands were labeled, in order of increasing size, as B7 to B11. The protein composition of each band is shown by the cartoon in the top right corners of Figure 3b–f. No single set of

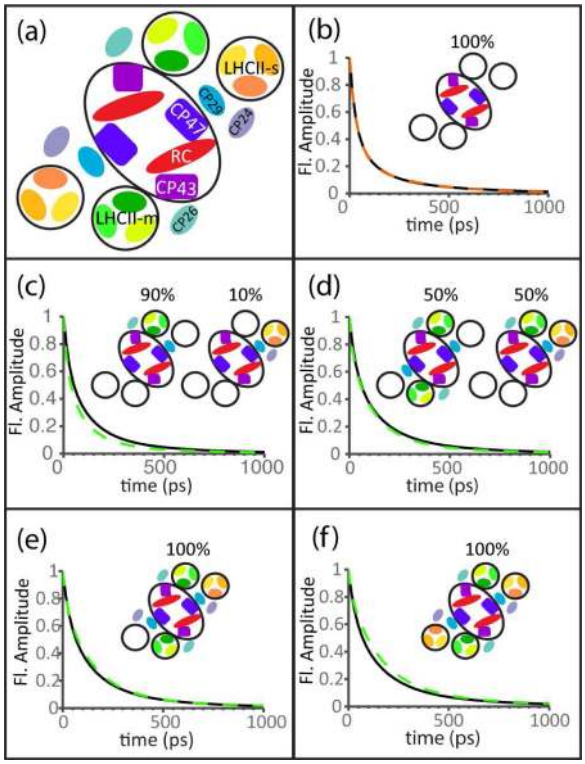

Figure 3. (a) A cartoon structure of PSII supercomplex proteins is shown. The contributions of different supercomplexes to each band are represented by similar cartoons in the top right corner of each panel. A comparison between experimental (black line, taken from Caffari and co-workers[3]) and simulated (orange and green dashed lines for B7 and B8–B11, respectively, calculated with the domain model) fluorescence decay curves for (b) B7, (c) B8, (d) B9, (e) B10, and (f) B11. The simulated decay curves are calculated using the best fit electron transfer time scales given in Table 1. The experimental curves discard the longest lifetime component following the work by Caffarri and co-workers (discussed in the Supporting Information).

electron transfer rates reasonably fits both the core complex (B7) and any of the larger supercomplexes simultaneously. As a result, two different sets of electron transfer time scales ($\tau = k^{-1}$) are shown in Table 1, one for the fit to the core complex data (B7) and the other for the fit to the data from the larger supercomplexes (B8–B11). The core complex data is described

Table 1. Best Fit Electron Transfer Time Scales for the Domain Model

	B8–B11	B7 (core complex)
τ_{CS} (ps)	0.64	4.4
τ_{RC} (ps)	160	130
τ_{irr} (ps)	520	250

by a much slower initial charge separation and faster irreversible electron/hole separation. The difference between the core and supercomplex electron transfer kinetics has been observed previously.[3] The origin, however, remains unclear: it could be an artifact of the modeling or the result of a physical difference in the samples not accounted for in the current structure/parameter data. In the following, we use the B8–B11 electron transfer rates to explore the dynamics of light harvesting in the largest supercomplex, $C_2S_2M_2$ (B11).

RESULTS AND DISCUSSION

Time Scales of Light Harvesting in $C_2S_2M_2$. The rate matrix provides a complete description of the kinetics of excitation energy and electron transfer, but a simplified picture would describe the average time scale for trapping in terms of contributions from a small set of effective forward transfer rates. The overall process of energy capture ($\tau_{capture}$), from initial excitation in the antenna to irreversible electron hole separation at the reaction center (RC), can be decomposed into four steps: (1) the diffusion of excitation energy among the antenna proteins until it reaches pigments that are kinetically connected to the RC (τ_{diff}), (2) excitation energy transfer into the RC (transfer to trap, τ_{TtT}), (3) excitation energy in the RC driving the initial charge separation (τ_{iCS}), and (4) the transfer of the electron downstream causing irreversible charge separation (τ_{irrCS}).[13,40] The breakdown of the overall time scale of capture into the component time scales is shown in eq 25.

$$\tau_{capture} = \tau_{diff} + \tau_{TtT} + \tau_{iCS} + \tau_{irrCS} \quad (25)$$

It is generally agreed that energy capture in PSII is limited by the rate of irreversible electron hole separation, which is 1–2 orders of magnitude slower that the other time scales involved.[7,9,38,41] We define light harvesting as the conversion of excitation energy to the initial charge separated state (RP1), which does not require irreversible charge separation. As such, light harvesting is described by only the first three time scales associated with energy capture ($\tau_{LH} = \tau_{diff} + \tau_{TtT} + \tau_{iCS}$). Previous work[7,9,42] has suggested that the kinetics of light harvesting in PSII are either trap limited ($\tau_{iCS} \gg \tau_{TtT} + \tau_{diff}$) or transfer-to-trap limited ($\tau_{TtT} \gg \tau_{iCS} + \tau_{diff}$). Knowledge of the rate limiting step would inform our interpretation of fluorescence lifetime data from both supercomplexes and intact membranes.[13,43]

One challenge in determining the relative contributions of τ_{diff}, τ_{TtT}, τ_{iCS}, and τ_{irrCS} is that they are not directly related to the rates of transfer in the rate matrix. These time scales describe the overall behavior of energy transport, which involves forward and reverse rates of transfer mixed with entropic effects (the connectivity of the different domains within the rate matrix). Yang and Fleming[21] have demonstrated a method that decomposes the average trapping time into contributions from different physical processes. In this treatment, a linear chain of kinetic compartments (σ_i), as shown in Figure 4, is constructed to reproduce the average time scale of capture. The kinetic compartments are linear

dx.doi.org/10.1021/ja403685a | J. Am. Chem. Soc. 2013, 135, 9164–9173

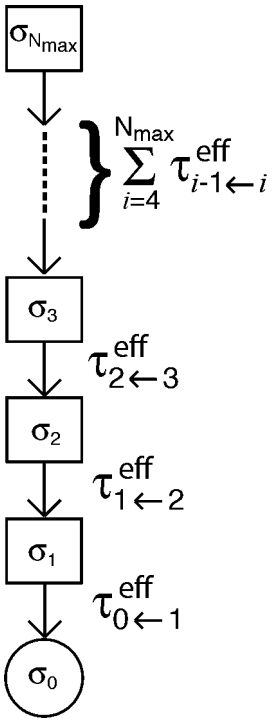

Figure 4. A diagram of the linear excitation energy cascade is shown where σ_0 represents RP2 in $C_2S_2M_2$. The effective time scales of transfer between kinetic compartments ($\tau^{\text{eff}}_{i-1\leftarrow i}$) is the average time of transfer from compartment i to $i-1$ averaging over all pathways starting at compartment i.

combinations of domains that form an orthonormal set. Excitation energy flows down the chain from the periphery of the supercomplex ($\sigma_{N_{\max}}$) to the final charge separation state RP2 (σ_0). The effective forward transition time ($\tau^{\text{eff}}_{i-1\leftarrow i}$, equation given in the Supporting Information) describes the time scale of transfer from σ_i to σ_{i-1} corrected for trajectories where excitation initially performs back transfer to higher compartments in the chain prior to transferring from σ_i to σ_{i-1}. These time scales, however, do not account for the initial distribution of excitation. A population-weighted effective transfer time ($t_{i-1\leftarrow i}$) weights $\tau^{\text{eff}}_{i-1\leftarrow i}$ for the population of excitation that will flow through compartment i and takes into account the initial excitation distribution (eqs 22−24). The most important advantage to the linear kinetic scheme described here is that the kinetic structure of the rate matrix is expressed in a form that can be related to the four steps of energy capture. For PSII, with the electron transfer scheme shown in Figure 2, τ_{TtT}, τ_{iCS}, and τ_{irrCS} are described by $t_{2\leftarrow 3}$, $t_{1\leftarrow 2}$, and $t_{0\leftarrow 1}$, respectively. τ_{diff} is described by a sum over the remaining time scales of transfer along the chain ($\sum_{n=4}^{N_{\max}} t_{n-1\leftarrow n}$).

The experimental fluorescence decay curves plotted in Figure 3 (black lines) have initial excitation evenly distributed among Chl-a molecules in the PSII supercomplexes. This is an important initial condition to consider, since most spectroscopic measurements of supercomplexes involve the excitation of a wide spatial distribution of chlorophylls. We have calculated the population-weighted effective transfer times for evenly distributed Chl-a excitation ($t^{\text{chlA}}_{i-1\leftarrow i}$), shown in Table 2. The contributions of different components to τ_{LH} break down as follows: 30% from τ_{diff}, 60% from τ_{TtT}, and 10% from τ_{iCS}. Given the similarity of the diffusion and transfer-to-trap contributions, when Chl-a molecules are evenly excited, light harvesting in $C_2S_2M_2$ should not be considered to occur in any of the previously suggested limits, though it is closer to the transfer-to-trap limit than any other.

Table 2. The Time Scales of Transfer in the $C_2S_2M_2$ Supercomplex Calculated Using the Effective Linearization Scheme in Figure 4

	assignments	t^{chlA} (ps)	$t^{\text{periphery}}$ (ps)[44]	description
τ_{irrCS}	$t_{0\leftarrow 1}$	560	560	RP2 ← RP1
τ_{iCS}	$t_{1\leftarrow 2}$	11	11	RP1 ← RC
τ_{TtT}	$t_{2\leftarrow 3}$	94	100	RC ← antenna
τ_{diff}	$\sum_{n=4}^{N_{\max}} t_{n-1\leftarrow n}$	50	110	diffusion in antenna

When a supercomplex resides within a membrane, a larger fraction of excitations will be initialized in the periphery of the supercomplex as a result of energy transfer from adjacent LHCII trimers or supercomplexes. This initial condition is quite different from those expected for measurements on isolated supercomplexes. Using our linearized kinetic model of PSII supercomplexes, however, we can explore the time scales of trapping associated with excitations entering from the edge of the supercomplex ($t^{\text{periphery}}_{i-1\leftarrow i}$). For peripheral excitations, τ_{diff} and τ_{TtT} each contribute approximately 50% of τ_{LH}. Incorporating additional energy transfer into and out of the domains contained in $C_2S_2M_2$, as a result of the additional pigments bound in the membrane, will increase both τ_{diff} and τ_{TtT}. It is likely, however, that τ_{diff} will increase more as the effective antenna size increases, and the average time scale for light harvesting will shift toward the diffusion limit.

SPATIAL ASPECTS OF LIGHT HARVESTING IN $C_2S_2M_2$

The overall efficiency of photoconversion depends on the energy transfer rates that arise from the combined energetic and spatial organization of chlorophyll in PSII supercomplexes. Our model shows no evidence of an energy funnel, in agreement with previous work on PSII antenna and core complex.[8,11] Studies of LHCII trimers have suggested that a low energy cluster of Chl-a's acts as a favored exit site.[14] Using the structure of PSII supercomplexes and considering the distances between chlorophyll, Caffarri and co-workers[16] have extended this thought by proposing that the exit site of LHCII-s should experience fast transport to a nearby pigment of CP43. A series of such rapid energy transfer steps could form a favored pathway from the peripheral LHCII trimers to the RC. Such a pathway would increase the photochemical yield by allowing excitation energy to reach a reaction center prior to loss by fluorescence or intersystem crossing. Using the domain model, we explore the appropriate description of the spatial distribution of energy flow through PSII supercomplexes.

We tested for the presence of favored energy transfer pathways in each quadrant of PSII. If a small number of such pathways exist, the photochemical yield should substantially decrease when one of these energy pathways is disrupted by removing an essential domain. We selected the two unique quadrants of $C_2S_2M_2$ as the subsystems of interest: the bottom right quadrant (RC, CP43, CP26, LHCII-s) and the top right quadrant (RC, CP47, CP29, CP24, LHCII-m), as shown in Figure 1a. We first calculated the photochemical yield of both subsystems. Subsequently, we performed a series of calculations of the photochemical yield for each subsystem in which one of the domains of the subsystem was removed. In all calculations, Chl-a's were evenly excited on the LHCII monomer farthest

dx.doi.org/10.1021/ja403685a | J. Am. Chem. Soc. 2013, 135, 9164−9173

from the RC. There was only one case where removing a domain reduced the photochemical yield to less than 85% of the photochemical yield of the intact subsystem. The one case corresponded to removing the 17 chlorophyll domains shared between CP47 and CP29, which removes all but one of the chlorophylls bound by CP47. This results in greatly suppressed photochemical yield, since, as can be seen in Figure 1b, the deletion of the large CP47 domain removes all chlorophyll in the vicinity of the reaction center. The general robustness to domain removal demonstrates that no single domain (excluding the 17 chlorophyll CP47 domains) is essential for efficient energy transfer to the reaction center. Instead, there are many energy transfer rates substantially faster than the time scale of loss (fluorescence and intersystem crossing), and this results in a collection of pathways that are fast enough to maintain high photochemical yield.

Next, we characterized how the time scale of light harvesting depends on a single spatial dimension, the average distance of the chlorophyll composing a domain to the nearest RC (d_{RC}). Figure 5 plots the average time scale for light harvesting (τ_{LH})

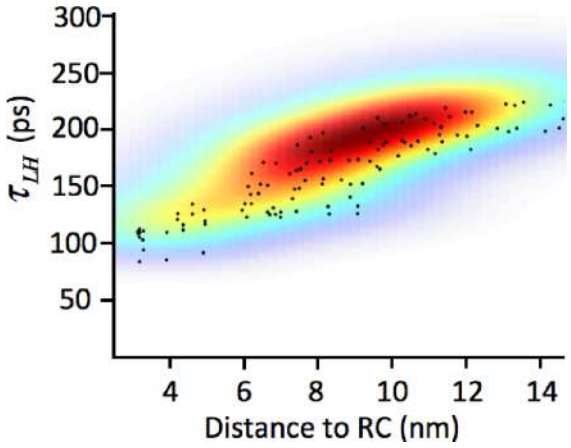

Figure 5. The time scale of light harvesting (τ_{LH}) for excitation initiated in each domain is plotted against the average distance from that domain to the nearest reaction center. The black dots denote the results from one inhomogeneous realization of the site energies. The colored contours (red indicating more points, blue indicating less) show the underlying distribution extracted from compartments calculated from 500 inhomogeneous realizations of the site energies. The underlying distribution was calculated with 2D Gaussian smoothing.

for excitation initiated in each domain against d_{RC}. The calculation of τ_{LH} for excitation initiated in a particular domain is equivalent to calculating the mean first passage time from that domain to the first radical pair state (RP1).[15] The dots represent the results of one calculation. The colored contours (with increasing density from blue to red) show the underlying distribution extracted from calculations with 500 realizations of the site energies. The overall process of light harvesting in PSII supercomplexes is insensitive to inhomogeneous realizations, as demonstrated by the similar width of the distributions for a single realization and for 500 realizations. Further, τ_{LH} for an excitation is linearly dependent on its distance to the nearest RC.

When a supercomplex is embedded in the grana membrane, it is surrounded by a dense array of pigment−protein complexes. A reaction center embedded in this array might be capable of efficiently capturing excitation energy initially absorbed far outside of the supercomplex it belongs to. Light harvesting is efficient anywhere that τ_{LH} is substantially smaller than the ∼2 ns time scale of excitation loss to unproductive pathways (fluorescence and intersystem crossing). The linear dependence shown in Figure 5 cannot be directly extended to a membrane, since the slope of the line will vary with the increased number of pigments and the unassociated LHCII may experience slower transport into the supercomplex than proteins bound by the supercomplex experience within it. However, the large disparity between the time scale of excitation loss (∼2 ns) and the ∼200 ps time scale of light harvesting found at the periphery of $C_2S_2M_2$ suggests that photosystem II reaction centers can efficiently harvest light from antenna assemblies much larger than that of $C_2S_2M_2$.

QUALITY OF FIT TO FLUORESCENCE DECAYS IS NOT A PROXY FOR ACCURACY OF ENERGY TRANSFER MODELS

Energy transfer models of PSII have typically been constructed by fitting kinetic models to fluorescence decay curves. The quality of fit has been used as an indicator of how well these kinetic models describe the underlying dynamics.[45,46] However, it may be that the fluorescence lifetime data, which is both ensemble averaged and averaged over all sites, is too coarse-grained to be able to distinguish between models with many fitting parameters.[9,47] We explored this possibility by simulating fluorescence lifetime curves using three different coarse-grain treatments of the domain model (Supporting Information, Figure 2) that correspond to kinetic limits that have been considered previously in the literature: (1) the ERPE model[7] assumes fast equilibration within all pigments of PSII, (2) the transfer-to-trap limited (TTL) model[9] assumes fast equilibration within the antenna pigments but slow transfer from the antenna to the RC (and vice versa), and (3) the protein model[3,38] assumes excitation equilibrates rapidly within a protein followed by slower transfer between proteins. Each of these models was constructed by coarse graining the domain model into compartments defined by regions of fast equilibration. The rates between compartments were calculated using eqs 13 and 14. None of these coarse-grained treatments quantitatively reproduced the population dynamics of the initial charge separated state (RP1) for $C_2S_2M_2$ calculated with the domain model. Despite any errors in reproducing the population dynamics of $C_2S_2M_2$, each of the three models is capable of simultaneously reproducing all four experimental fluorescence decay curves measured for the B8−B11 bands of PSII supercomplexes if we allow the three electron transfer parameters to vary. The time constants that describe electron transfer for the best simultaneous fit to bands B8−B11 for each model are shown in Table 3, and the root-mean-square error (RMSE) is reproduced in the last row. The electron transfer rates extracted for each model vary significantly from the

Table 3. The Best Fit Electron Transfer Time Scales for the Domain, Protein, Transfer-to-Trap Limited, and ERPE Models

B8−B11	domain	protein	TTL	ERPE
τ_{CS} (ps)	0.64	2.1	2.2	0.28
τ_{RC} (ps)	160	140	91	1.0
τ_{irr} (ps)	520	260	190	33
RMSE ($\times 10^{-2}$)	1.7	1.6	1.4	1.9

dx.doi.org/10.1021/ja403685a | J. Am. Chem. Soc. 2013, 135, 9164−9173

domain model results, simply because the energy transfer rates describe substantially different dynamics. The quality of the fits (as reported by the RMSE), however, is very similar to that produced by the domain model. Therefore, a model with a good fit to fluorescence lifetime data does not necessarily describe the energy transfer dynamics correctly. The electron transfer rates extracted from such a fit will not accurately describe the kinetics of electron hole separation in reaction centers. More generally, caution should be taken when making mechanistic claims based on fitting kinetic models to fluorescence decay data.

CONCLUSIONS

An accurate model of energy transfer in PSII and grana membranes is necessary for the proper interpretation of chlorophyll fluorescence measurements, which are widely used to study photosynthesis.[48] Detailed models of energy transfer have been developed for several components of PSII.[8,11,28] We have constructed the first structure-based model of light harvesting in assemblies of antenna proteins and RCs larger than the core complex, the PSII supercomplexes. The model describes how the specific arrangement of light harvesting proteins and pigments gives rise to efficient energy capture and the fluorescence lifetimes previously measured by Caffarri and co-workers.[3] This model can be used to put lower bounds on energy transfer time scales in the membrane. We also anticipate extending this model to explicitly treat energy transfer through the grana membrane by combining the current structural data of PSII and LHCII with images[2] and simulations[49] of protein organization in the grana.

In developing a structure-based model of energy transfer and trapping in PSII supercomplexes, we used a new metric for defining kinetic domains which improves the separation of time scales between intra- and interdomain transfer rates. The results from analyzing our model of energy transfer in photosystem II supercomplexes are as follows:

(1) The domain model is the most coarse-grained model that quantitatively reproduces the energy transfer dynamics of $C_2S_2M_2$ calculated with the full modified Redfield/generalized Förster rate matrix.

(2) A linearized kinetic model of trapping showed that the time scale for light harvesting in $C_2S_2M_2$ is not well described by any limiting case but is primarily due to a combination of the diffusion and transfer-to-trap rates in the light harvesting antenna. The longer time scales of diffusion experienced by excitations initiated on the periphery of $C_2S_2M_2$ suggest that the time scale for light harvesting in grana membranes shifts toward the diffusion limit.

(3) Analyzing the sensitivity of the photochemical yield of $C_2S_2M_2$ to the removal of domains has demonstrated that there is not a small set of favored energy transfer pathways that are required for efficient energy transport and capture in PSII supercomplexes. Therefore, the efficiency of energy capture is created by many rates of energy transfer between domains of chlorophyll that are much faster than the rates of excitation quenching by loss pathways such as intersystem crossing and fluorescence.

(4) The time scale for light harvesting of an excitation was shown to depend linearly on its distance to the nearest reaction center. On the basis of this trend, the capture radius of PSII RC in the grana membrane is significantly larger than the 15 nm maximum distance to a RC achieved in $C_2S_2M_2$.

(5) Energy transfer models that do not correctly treat population dynamics within PSII supercomplexes can still fit the measured fluorescence decay curves. The resulting electron transfer rates, however, do not accurately describe electron/hole separation in the reaction center.

ASSOCIATED CONTENT

Supporting Information

The Hamiltonian parameters, additional comments, and figures related to coarse-grain modeling of PSII. This material is available free of charge via the Internet at http://pubs.acs.org.

AUTHOR INFORMATION

Corresponding Author

fleming@cchem.berkeley.edu

Notes

The authors declare no competing financial interest.

ACKNOWLEDGMENTS

D.I.G.B would like to thank Vladimir Novoderezhkin for helpful discussions about modified Redfield and LHCII calculations, Mino Yang for discussion of linearized kinetic models, and Rienk van Grondelle for helpful discussions. D.I.G.B. and K.A. would like to thank Roberta Croce for providing her structure of the $C_2S_2M_2$ supercomplex and Julia Zaks, Eleonora De Re, and Emily Jane Sylak-Glassman for extensive comments on the manuscript. K.A. was partially supported by a National Science Foundation Graduate Research Fellowship. This work was supported by the Director, Office of Science, Office of Basic Energy Sciences, of the US Department of Energy under Contract DEAC02-05CH11231 and the Division of Chemical Sciences, Geosciences, and Biosciences, Office of Basic Energy Sciences of the US Department of Energy through Grant DE-AC03-76SF000098.

REFERENCES

(1) Dekker, J.; Boekema, E. *Biochim. Biophys. Acta, Bioenerg.* **2005**, *1706*, 12−39.
(2) Kouřil, R.; Dekker, J. P.; Boekema, E. J. *Biochim. Biophys. Acta, Bioenerg.* **2012**, *1817*, 2−12.
(3) Caffarri, S.; Broess, K.; Croce, R.; van Amerongen, H. *Biophys. J.* **2011**, *100*, 2094−2103.
(4) Ruban, A. V.; Johnson, M. P.; Duffy, C. D. P. *Biochim. Biophys. Acta, Bioenerg.* **2012**, *1817*, 167−181.
(5) Jahns, P.; Holzwarth, A. R. *Biochim. Biophys. Acta, Bioenerg.* **2012**, *1817*, 182−193.
(6) Minagawa, J. *Biochim. Biophys. Acta, Bioenerg.* **2011**, *1807*, 897−905.
(7) Miloslavina, Y.; Szczepaniak, M.; Müller, M. G.; Sander, J.; Nowaczyk, M.; Rögner, M.; Holzwarth, A. R. *Biochemistry* **2006**, *45*, 2436−42.
(8) Raszewski, G.; Renger, T. *J. Am. Chem. Soc.* **2008**, *130*, 4431−4446.
(9) van der Weij-de Wit, C. D.; Dekker, J. P.; van Grondelle, R.; van Stokkum, I. H. M. *J. Phys. Chem. A* **2011**, *115*, 3947−3956.
(10) Blankenship, R. E. *Molecular Mechanisms of Photosynthesis*; Blackwell Publishing: Malden, MA, 2002.
(11) Novoderezhkin, V.; Marin, A.; van Grondelle, R. *Phys. Chem. Chem. Phys.* **2011**, *13*, 17093−17103.
(12) Broess, K.; Trinkunas, G.; van Hoek, A.; Croce, R.; van Amerongen, H. *Biochim. Biophys. Acta, Bioenerg.* **2008**, *1777*, 404−409.
(13) Croce, R.; van Amerongen, H. *J. Photochem. Photobiol., B* **2011**, *104*, 142−153.

(14) Schlau-Cohen, G. S.; Calhoun, T. R.; Ginsberg, N. S.; Read, E. L.; Ballottari, M.; Bassi, R.; van Grondelle, R.; Fleming, G. R. *J. Phys. Chem. B* **2009**, *113*, 15352−15363.
(15) Park, S.; Sener, M.; Lu, D.; Schulten, K. *J. Chem. Phys.* **2003**, *119*, 1313−1319.
(16) Caffarri, S.; Kouril, R.; Kereiche, S.; Boekema, E. J.; Croce, R. *EMBO J.* **2009**, *28*, 3052−3063.
(17) Novoderezhkin, V. I.; Palacios, M. A.; van Amerongen, H.; van Grondelle, R. *J. Phys. Chem. B* **2005**, *109*, 10493−10504.
(18) Müh, F.; Madjet, M. E.-A.; Renger, T. *J. Phys. Chem. B* **2010**, *114*, 13517−13535.
(19) Renger, T.; Madjet, M. E.; Knorr, A.; Müh, F. *J. Plant Physiol.* **2011**, *168*, 1497−1509.
(20) Müh, F.; Renger, T. *Biochim. Biophys. Acta, Bioenerg.* **2012**, *1817*, 1446−1460.
(21) Yang, M.; Fleming, G. R. *J. Chem. Phys.* **2003**, *119*, 5614−5622.
(22) Ishizaki, A.; Calhoun, T. R.; Schlau-Cohen, G. S.; Fleming, G. R. *Phys. Chem. Chem. Phys.* **2010**, *12*, 7319−7337.
(23) Umena, Y.; Kawakami, K.; Shen, J.-R.; Kamiya, N. *Nature* **2011**, *473*, 55−60.
(24) Liu, Z.; Yan, H.; Wang, K.; Kuang, T.; Zhang, J.; Gui, L.; An, X.; Chang, W. *Nature* **2004**, *428*, 287−292.
(25) Pan, X.; Li, M.; Wan, T.; Wang, L.; Jia, C.; Hou, Z.; Zhao, X.; Zhang, J.; Chang, W. *Nat. Struct. Mol. Biol.* **2011**, *18*, 309−315.
(26) Lomize, M. A.; Lomize, A. L.; Pogozheva, I. D.; Mosberg, H. I. *Bioinformatics* **2006**, *22*, 623−625.
(27) Humphrey, W.; Dalke, A.; Schulten, K. *J. Mol. Graphics* **1996**, *14*, 33−38.
(28) Müh, F.; Madjet, M. E.-A.; Renger, T. *Photosynth. Res.* **2012**, *111*, 87−101.
(29) Raszewski, G.; Diner, B. A.; Schlodder, E.; Renger, T. *Biophys. J.* **2008**, *95*, 105−19.
(30) Raszewski, G.; Saenger, W.; Renger, T. *Biophys. J.* **2005**, *88*, 986−98.
(31) Madjet, M. E.; Abdurahman, A.; Renger, T. *J. Phys. Chem. B* **2006**, *110*, 17268−17281.
(32) Krueger, B. P.; Scholes, G. D.; Fleming, G. R. *J. Phys. Chem. B* **1998**, *102*, 5378−5386.
(33) Novoderezhkin, V. I.; Romero, E.; Dekker, J. P.; van Grondelle, R. *ChemPhysChem* **2011**, *12*, 681−688.
(34) Belyaeva, N. E.; Schmitt, F. J.; Steffen, R.; Paschenko, V. Z.; Riznichenko, G. Y.; Chemeris, Y. K.; Renger, G.; Rubin, A. B. *Photosynth. Res.* **2008**, *98*, 105−119.
(35) Palacios, M.; de Weerd, F.; Ihalainen, J.; van Grondelle, R.; van Amerongen, H. *J. Phys. Chem. B* **2002**, *106*, 5782−5787.
(36) Zhu, X.; Govindjee; Baker, N.; deSturler, E.; Ort, D.; Long, S. *Planta* **2005**, *223*, 114−133.
(37) Yang, M.; Damjanovic, A.; Vaswani, H.; Fleming, G. *Biophys. J.* **2003**, *85*, 140−158.
(38) Broess, K.; Trinkunas, G.; van der Weij-de Wit, C. D.; Dekker, J. P.; van Hoek, A.; van Amerongen, H. *Biophys. J.* **2006**, *91*, 3776−3786.
(39) Valkunas, L.; Chmeliov, J.; Trinkunas, G.; Duffy, C. D. P.; van Grondelle, R.; Ruban, A. V. *J. Phys. Chem. B* **2011**, *115*, 9252−9260.
(40) van Amerongen, H.; Valkunas, L.; van Grondelle, R. *Photosynthetic Excitons*; World Scientific: Singapore, 2000.
(41) Groot, M. L.; Pawlowicz, N. P.; van Wilderen, L. J. G. W.; Breton, J.; van Stokkum, I. H. M.; Grondelle, R. V. *Proc. Natl. Acad. Sci. U.S.A.* **2005**, *102*, 13087−92.
(42) van Oort, B.; Alberts, M.; de Bianchi, S.; Dall'Osto, L.; Bassi, R.; Trinkunas, G.; Croce, R.; van Amerongen, H. *Biophys. J.* **2010**, *98*, 922−931.
(43) Renger, T.; Schlodder, E. *ChemPhysChem* **2010**, *11*, 1141−1153.
(44) Since excitations on the periphery of $C_2S_2M_2$ are contained by the highest compartment of the chain, the population weighting of all effective rates of transfer (ρ_i, given in eq 24) will equal 1 and $t_{i-1\leftarrow i}^{\text{periphery}} = \tau_{i-1\leftarrow i}^{\text{eff}}$.
(45) Holzwarth, A. R. In *Biophysical Techniques in Photosynthesis*; Amesz, J., Hoff, A. J., Eds.; Kluwer Academic Publishers: Dordrecht, The Netherlands, 1996; pp 75−92.
(46) van Stokkum, I. H. M.; Larsen, D. S.; van Grondelle, R. *Biochim. Biophys. Acta, Bioenerg.* **2004**, *1657*, 82−104.
(47) Tian, L.; Farooq, S.; van Amerongen, H. *Phys. Chem. Chem. Phys.* **2013**, *15*, 3146−3154.
(48) Papageorgiu, G. C., Govindjee, Eds. *Chlorophyll a Fluorescence: A Signature of Photosynthesis*; Advances in Photosynthesis and Respiration, Vol. *19*; Springer: Dordrecht, The Netherlands, 2004.
(49) Schneider, A. R.; Geissler, P. L. Preprint, 2013, arXiv/1302.6323v1 [cond-mat.soft].

NOTE ADDED AFTER ASAP PUBLICATION

The Abstract graphic and Figures 2, 4, and 5 have been updated. The revised version was re-posted on June 10, 2013.